Nuclear Magnetic Resonance Coherence-Order- and Spin-State-Selective Correlation in I_2S Spin Systems

T. S. Untidt,[†] T. Schulte-Herbrüggen,[‡] O. W. Sørensen,[‡] and N. C. Nielsen*,[†]

Laboratory for Biomolecular NMR Spectroscopy, Department of Molecular and Structural Biology, University of Aarhus, DK-8000 Aarhus C, Denmark, and Department of Chemistry, Carlsberg Laboratory, Gamle Carlsberg Vej 10, DK-2500 Valby, Denmark

Received: March 19, 1999

We present coherence-order- and spin-state-selective (COS^3) HSQC pulse sequences for $2(I_{1z} + I_{2z})S^- \rightarrow I_1^- I_2^{\alpha/\beta} + I_1^{\alpha/\beta} I_2^-$ and $S^- \rightarrow I_1^- I_2^{\alpha/\beta} + I_1^{\alpha/\beta} I_2^-$ transfer in I_2S spin systems. The sequences provide the theoretical maximum transfer efficiency and improved effective resolution in the *I*-spin dimension and allow for heteronuclear gradient echoes without loss in sensitivity. For the antiphase transfer the sensitivity is improved by 41% relative to the previous spin-state-selective α&β-HSQC experiment, while the in-phase sequence is the first of its kind. In the regime of well-separated *J* doublet lines, the sensitivity enhancement amounts to 100% and 65% relative to previous antiphase and in-phase coherence-order-selective experiments, respectively. The new COS^3 HSQC experiments and previous methods are compared experimentally using β-*O*-methyl maltoside.

1. Introduction

Recent years have witnessed great interest in multidimensional NMR experiments providing the highest achievable sensitivity and spectra with the simplest possible multiplet patterns containing the desired spectral information. Distribution of the intensity on fewer peaks generally improves the sensitivity and the effective resolution, which in turn can make visible small coupling constants otherwise buried in complex multiplet patterns. Hence, the demands of sensitivity optimization and multiplet simplification often go hand in hand and form an important element in a systematic strategy for experimental design. Recently this was demonstrated by a double- to single-quantum transfer scheme[1−3] which doubles the sensitivity of the INADEQUATE experiment[4,5] by directing coherence transfer from, e.g., $I_1^- I_2^-$ entirely into $I_1^- I_2^\beta + I_1^\beta I_2^-$. This transfer is selective with respect to both coherence order (only antiecho peaks) and spin state (only β peaks) and is referred to as coherence-order- and spin-state-selective (COS^3) transfer. Another example in this category is double spin-state-selective coherence transfer.[6] In other cases, efficient experiments have focused on either coherence-order-selective (COS)[7−10] or spin-state-selective (S^3)[11−16] transfer. What is optimum depends on the resolution demand of the experiment, the relevant coherence transfer, and specific needs such as formation of heteronuclear coherence transfer echoes by pulsed field gradients (PFG) for artifact suppression. Several of these experiments provide optimum efficiency according to unitary bounds on spin dynamics.[17−22]

α&β-HSQC[11] represents an example of an S^3 experiment which, although improving the effective resolution and the sensitivity relative to the COS variant,[7] will benefit substantially by turning it into a COS^3 variant. This experiment is of interest for resolution-enhanced $^1H-^{13}C$ correlation spectroscopy and for measurement of geminal $^1H-^1H$ *J* and dipolar coupling constants in I_2S spin systems. In the original α&β-HSQC experiment $2F_zS^\pm \rightarrow I_1^- I_2^{\alpha/\beta} + I_1^{\alpha/\beta} I_2^-$ ($F_z = I_{1z} + I_{2z}$) transfer was obtained by combination of echo and antiecho spectra out of two data sets. In this paper we derive COS^3 mixing sequences accomplishing one of the specific transfers

$$2F_zS^- \rightarrow I_1^- I_2^{\alpha/\beta} + I_1^{\alpha/\beta} I_2^- \tag{1}$$

or

$$S^- \rightarrow I_1^- I_2^{\alpha/\beta} + I_1^{\alpha/\beta} I_2^- \tag{2}$$

with optimum sensitivity.

2. Systematic Design of Optimum COS^3 Experiments

Our strategy for systematic design of optimum pulse sequences involves (i) definition of the appropriate initial (*A*) and target (*C*) operators with the desired properties, (ii) determination of the theoretically largest efficiency for conversion of *A* into *C* which serves as a standard to which trial experiments are compared, and based on this (iii) derivation of experiments which achieve the maximum transfer efficiency.

The transformation between *A* and *C* is described by

$$UAU^\dagger = b(U)C + Q, \quad Tr\{C^\dagger Q\} = 0 \tag{3}$$

where *U* is the unitary propagator representing the experiment (ignoring relaxation and other dissipative processes) and

$$b(U) = \frac{Tr\{C^\dagger UAU^\dagger\}}{Tr\{C^\dagger C\}} \tag{4}$$

the corresponding transfer efficiency. The maximum transfer

* To whom correspondence should be addressed. Fax: +4586 196199. Tel: +4589 423841. E-mail: ncn@kemi.aau.dk.
[†] University of Aarhus.
[‡] Carlsberg Laboratory.

10.1021/jp990968l CCC: $18.00
Published on Web 10/22/1999

TABLE 1: Unitary Bounds ($(b_{max})^{sym}$), Norm Bounds (b_{max}^{norm}), and Efficiencies of Previous Experiments (b_{exp}) for the Coherence-Transfer Processes Described in Eqs 1 and 2 Assuming Permutation Symmetric Perturbations

transfer	$(b_{max})^{sym}$	b_{max}^{norm}	b_{exp}
$2F_zS^- \rightarrow I_1^- I_2^{\alpha/\beta} + I_1^{\alpha/\beta} I_2^-$	$\sqrt{2}$ (1.4142)	$\sqrt{2}$	1
$S^- \rightarrow I_1^- I_2^{\alpha/\beta} + I_1^{\alpha/\beta} I_2^-$	$1/\sqrt{2}$ (0.7071)	1	–

efficiency, i.e., the so-called unitary bound value

$$b_{max} = \max_U |b(U)| \tag{5}$$

can be determined numerically for arbitrary initial and target operators using an iterative algorithm searching for the zero value of the gradient[21]

$$\nabla|b(U)|^2 = \{(b^*(U)[UA^\dagger U^\dagger,C])^\dagger - b^*(U)[UA^\dagger U^\dagger,C]\}U \tag{6}$$

To determine b_{max} and design practically useful experiments, it is relevant to consider possible constraints in the propagators. In particular, it is of interest to focus on nonselective pulse sequences implying that the perturbation be invariant to permutation of the spins of the same kind. For the I_2S experiments in mind, this restricts operations to I-spin permutation symmetric Hamiltonians and this may reduce the maximum transfer efficiency[20,21] relative to the value applying in the absence of permutation symmetry, i.e.,

$$(b_{max})^{sym} \leq b_{max} \tag{7}$$

Furthermore, to keep the pulse sequence short, the external manipulations should not rely on the rather weak coupling between the two I spins. In the present case, this does not reduce the unitary bound values any further.[22] The unitary bounds for the transfers in eqs 1 and 2 are listed in Table 1 along with the efficiencies of previous spin-state-selective experiments[11] and those predicted by conservation of the norm for the density operator,[23]

$$b_{max}^{norm} = \sqrt{\frac{Tr\{A^\dagger A\}}{Tr\{C^\dagger C\}}} \tag{8}$$

Two features should be noted: (i) the state-of-the-art S^3 $\alpha\&\beta$-HSQC experiment may be improved by 41% for the antiphase transfer while no experiment exists for the in-phase transfer and (ii) for the antiphase transfer the maximum transfer efficiency equals that predicted by norm conservation. The latter fact indicates that the entire initial coherence can be transferred into the target state (i.e., there is no residual term Q) for this transfer.

I-spin permutation symmetric perturbations invite a coupled representation spanned by the basis functions

$$|1\rangle = |\alpha\alpha\rangle|\alpha\rangle \qquad |2\rangle = |\alpha\alpha\rangle|\beta\rangle$$

$$|3\rangle = \frac{1}{\sqrt{2}}\{|\alpha\beta\rangle + |\beta\alpha\rangle\}|\alpha\rangle \qquad |4\rangle = \frac{1}{\sqrt{2}}\{|\alpha\beta\rangle + |\beta\alpha\rangle\}|\beta\rangle$$

$$|5\rangle = |\beta\beta\rangle|\alpha\rangle \qquad |6\rangle = |\beta\beta\rangle|\beta\rangle$$

$$|7\rangle = \frac{1}{\sqrt{2}}\{|\alpha\beta\rangle - |\beta\alpha\rangle\}|\alpha\rangle \qquad |8\rangle = \frac{1}{\sqrt{2}}\{|\alpha\beta\rangle - |\beta\alpha\rangle\}|\beta\rangle \tag{9}$$

where $|m_1m_2\rangle|m_3\rangle$ ($|m_i\rangle = |\alpha\rangle$ or $|\beta\rangle$) are Zeeman basis functions with the spins ordered I_1, I_2, and S. Within this basis, the operators in eqs 1 and 2 take the form

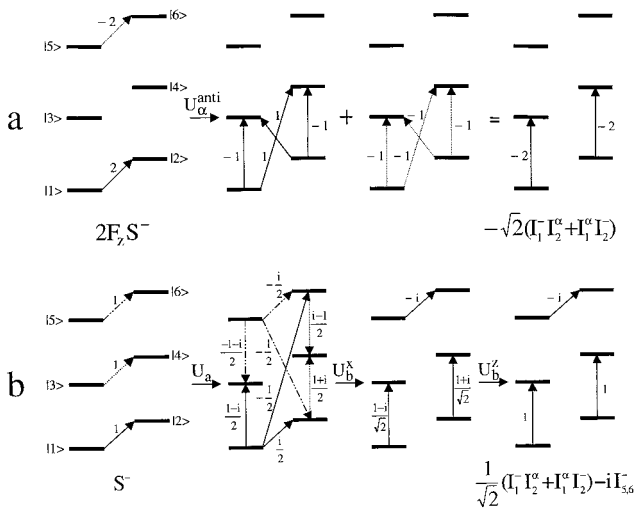

Figure 1. Energy-level diagrams illustrating the initial (left column) and final (right column) operators (coupled representation) involved in (a) $2F_zS^- \rightarrow I_1^- I_2^\alpha + I_1^\alpha I_2^-$ and (b) $S^- \rightarrow I_1^- I_2^\alpha + I_1^\alpha I_2^-$ coherence transfer in I_2S spin systems with equivalent I spins. The optimum propagators (a) U_α^{anti} and (b) $U_\alpha^{in} = U_b^z U_b^x U_a$ are defined in the text.

$$2F_zS^- = 2\{I_{1,2}^- - I_{5,6}^-\} \tag{10}$$

$$S^- = I_{1,2}^- + I_{3,4}^- + I_{5,6}^- + I_{7,8}^- \tag{11}$$

$$I_1^- I_2^\alpha + I_1^\alpha I_2^- = \sqrt{2}\{I_{1,3}^- + I_{2,4}^-\} \tag{12}$$

$$I_1^- I_2^\beta + I_1^\beta I_2^- = \sqrt{2}\{I_{3,5}^- + I_{4,6}^-\} \tag{13}$$

where $I_{r,s}^- = |s\rangle\langle r|$ is a single-element operator.[24,25] Confining the experiments to nonselective rotations, the effective part of U is restricted to the 6×6 block corresponding to a total I-spin angular momentum of $I = 1$.

Representation of the initial and target operators in an energy-level diagram in accordance with the symmetry of the perturbations (Figure 1) is useful in the design of optimum pulse sequences. In favorable cases, this allows immediate identification of optimum selective rotations which can be transformed into nonselective experiments.[2,6,10,17] In less favorable cases, the diagrams reveal that optimum transfer requires more complicated transformations possibly involving noncommuting rotations. Consider, for example, $2F_zS^- \rightarrow I_1^- I_2^\alpha + I_1^\alpha I_2^-$ where a π rotation under the heteronuclear zero-quantum (ZQ) operator $(I_x^{2,3} + I_x^{4,5} = (2F_xS_x + 2F_yS_y)/2\sqrt{2})$[10] transforms $2F_zS^-$ into $-2i(I_{1,3}^- - I_{4,6}^-)$. $I_{1,3}^-$ is part of the target operator while $I_{4,6}^-$ would require a subsequent I-spin double-quantum (2Q) rotation acting selectively on operators with S in the β state in order to be converted into the desired $I_{2,4}^-$ operator of the target state. This is not straightforward when relying only on heteronuclear couplings. Consequently, it may be more rewarding to consider alternative strategies, for example, involving operators of the type $2F_yS_y$ and F_xS^β,[11] to distribute the initial coherences into several coherences which subsequently are transformed into the target operator. Participation of more coherences and potentially non-commuting transformations, however, makes it exceedingly difficult to design highly selective experiments solely on the basis of the energy-level diagrams. In the following we demonstrate that these may conveniently be derived by numerical optimization.

In the search for optimum transformations, we need the transfer functions which for the four relevant transfers according to eq 4 take the form

$$b_{\alpha}^{\mathrm{anti}}(U) = \frac{1}{\sqrt{2}}(u_{11}^{*}u_{32} + u_{21}^{*}u_{42} - u_{15}^{*}u_{36} - u_{25}^{*}u_{46}) \quad (14)$$

$$b_{\beta}^{\mathrm{anti}}(U) = \frac{1}{\sqrt{2}}(u_{31}^{*}u_{52} - u_{35}^{*}u_{56} + u_{41}^{*}u_{62} - u_{45}^{*}u_{66}) \quad (15)$$

$$b_{\alpha}^{\mathrm{in}}(U) = \frac{1}{2\sqrt{2}}(u_{11}^{*}u_{32} + u_{13}^{*}u_{34} + u_{21}^{*}u_{42} + u_{23}^{*}u_{44} + u_{15}^{*}u_{36} + u_{25}^{*}u_{46}) \quad (16)$$

$$b_{\beta}^{\mathrm{in}}(U) = \frac{1}{2\sqrt{2}}(u_{31}^{*}u_{52} + u_{33}^{*}u_{54} + u_{35}^{*}u_{56} + u_{41}^{*}u_{62} + u_{43}^{*}u_{64} + u_{45}^{*}u_{66}) \quad (17)$$

where $u_{ij} = \langle i|Uj\rangle$. The superscripts anti and in refer to antiphase (eq 1) and in-phase (eq 2) transfers, respectively, while the greek subscript denotes the state of the passive spin in the target operators. We note that for, e.g., the $2F_zS^- \rightarrow I_1^- I_2^{\alpha} + I_1^{\alpha} I_2^-$ transfer the elements u_{11}, u_{21}, u_{32}, and u_{42} alone are responsible for transfer of $I_{1,2}^-$ into $I_{1,3}^- + I_{2,4}^-$, while the elements u_{15}, u_{25}, u_{36}, and u_{46} are responsible for the transfer starting from $I_{5,6}^-$.

Using eqs 14−17 and an appropriate set of experimentally feasible propagators (pulses and delays or more advanced pulse sequence elements), it is straightforward to optimize $b(U)$ against the maximum transfer efficiency $(b_{\max})^{\mathrm{sym}}$ to derive optimum pulse sequences. The propagators corresponding to the shortest optimum COS^3 pulse sequences found are

$$U_{\alpha}^{\mathrm{anti}} = \mathrm{e}^{-i(\pi/2)2F_yS_x}\mathrm{e}^{i(\pi/2-\theta_m)2F_zS_y}\mathrm{e}^{-i(2\pi/3)F_yS^{\beta}}\mathrm{e}^{i\theta_m 2F_zS_y}\mathrm{e}^{-i(\pi/4)F_y} \quad (18)$$

$$U_{\beta}^{\mathrm{anti}} = \mathrm{e}^{-i(\pi/2)2F_yS_x}\mathrm{e}^{-i(\pi/2-\theta_m)2F_zS_y}\mathrm{e}^{i(2\pi/3)F_yS^{\alpha}}\mathrm{e}^{-i\theta_m 2F_zS_y}\mathrm{e}^{i(\pi/4)F_y} \quad (19)$$

$$U_{\alpha}^{\mathrm{in}} = \mathrm{e}^{-i(\pi/2)2F_yS_y}\mathrm{e}^{-i(\pi/2-\theta_m)2F_yS_x}\mathrm{e}^{i(2\pi/3)F_zS^{\beta}}\mathrm{e}^{-i\theta_m 2F_yS_x} \quad (20)$$

$$U_{\beta}^{\mathrm{in}} = \mathrm{e}^{-i(\pi/2)2F_yS_y}\mathrm{e}^{i(\pi/2-\theta_m)2F_yS_x}\mathrm{e}^{-i(2\pi/3)F_zS^{\alpha}}\mathrm{e}^{i\theta_m 2F_yS_x} \quad (21)$$

where $\theta_m = \tan^{-1}(\sqrt{2})$ denotes the magic angle. Within the coupled basis, the four propagators may be described by the relevant $I = 1$ 6×6 matrix representations ($q = 1/\sqrt{2}$ and $p = {}^1/_2(1 + i)$)

$$U_{\alpha}^{\mathrm{anti}} = \begin{bmatrix} q & 0 & 0 & 0 & q & 0 \\ -q & 0 & 0 & 0 & q & 0 \\ 0 & -q & 0 & 0 & 0 & q \\ 0 & q & 0 & 0 & 0 & q \\ 0 & 0 & 0 & -1 & 0 & 0 \\ 0 & 0 & 1 & 0 & 0 & 0 \end{bmatrix},$$

$$U_{\beta}^{\mathrm{anti}} = \begin{bmatrix} 0 & 0 & 0 & -1 & 0 & 0 \\ 0 & 0 & 1 & 0 & 0 & 0 \\ q & 0 & 0 & 0 & q & 0 \\ -q & 0 & 0 & 0 & q & 0 \\ 0 & -q & 0 & 0 & 0 & q \\ 0 & q & 0 & 0 & 0 & q \end{bmatrix} \quad (22)$$

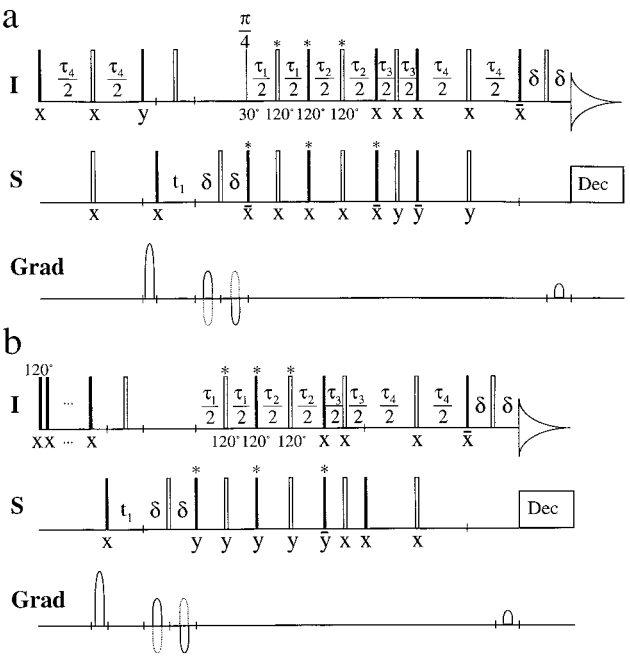

Figure 2. Pulse sequences for (a) $2F_zS^- \rightarrow I_1^- I_2^{\alpha/\beta} + I_1^{\alpha/\beta} I_2^-$ and (b) $S^- \rightarrow I_1^- I_2^{\alpha/\beta} + I_1^{\alpha/\beta} I_2^-$ COS^3 HSQC experiments for I_2S spin systems. Unless stated otherwise above the pulses, open and filled bars represent π and $\pi/2$ pulses. The pulse phases applying for transfer into the α resonances are given below the pulses; the phase for pulses marked by an asterisk must be reversed for transfer into the β resonances. The delays are related to the one-bond heteronuclear J_{CH} coupling constant as $\tau_1 = \theta_m(\pi J_{\mathrm{CH}})^{-1}$, $\tau_2 = (3J_{\mathrm{CH}})^{-1}$, $\tau_3 = (\pi/2 - \theta_m)(\pi J_{\mathrm{CH}})^{-1}$, and $\tau_4 = (2J_{\mathrm{CH}})^{-1}$, where $\theta_m = \tan^{-1}(\sqrt{2})$ is the magic angle.

TABLE 2: Transfer Amplitudes $|b(U)|$ for *IS* and I_3S Spin Systems Using the Various I_2S HSQC Experiments

spin system	transfer	COS^3	S^3	COS	$(b_{\max})^{\mathrm{sym}}$
IS	$2I_zS^- \rightarrow I^-$	0.805	0.500	0.896	1
	$S^- \rightarrow I^-$	0.739	0.250	0.675	1
I_3S	$2F_zS^- \rightarrow F^-$	0.475	0.500	0.592	0.744
	$S^- \rightarrow F^-$	0.174	0	0.310	0.455

$$U_{\alpha}^{\mathrm{in}} = \begin{bmatrix} p & 0 & 0 & 0 & p^* & 0 \\ 0 & 0 & -i & 0 & 0 & 0 \\ 0 & p & 0 & 0 & 0 & p^* \\ 0 & 0 & 0 & -i & 0 & 0 \\ p^* & 0 & 0 & 0 & p & 0 \\ 0 & -p^* & 0 & 0 & 0 & -p \end{bmatrix},$$

$$U_{\beta}^{\mathrm{in}} = \begin{bmatrix} -p & 0 & 0 & 0 & p^* & 0 \\ 0 & p & 0 & 0 & 0 & -p^* \\ 0 & 0 & -i & 0 & 0 & 0 \\ p^* & 0 & 0 & 0 & -p & 0 \\ 0 & 0 & 0 & i & 0 & 0 \\ 0 & -p^* & 0 & 0 & 0 & p \end{bmatrix} \quad (23)$$

which (according to eqs 5 and 14−17) provide the maximum efficiencies defined by the unitary bound on spin dynamics (cf. Table 1). Using standard transformations, the four propagators are readily expressed in terms of the mixing part of the HSQC pulse sequences given in Figure 2. Table 2 compares transfer amplitudes for *IS* and I_3S spin systems subjected to the various antiphase and in-phase COS, S^3, and COS^3 HSQC pulse sequences.

With the optimum pulse sequences derived, it is instructive to describe the transformation of the various coherences between the initial and target spin states. It turns out that this is easiest

for the in-phase sequences. Consider, for example, the in-phase α COS^3 sequence for which the relevant Hamiltonians in terms of single-transition operators in the coupled basis read

$$2F_yS_y = \sqrt{2}\{(I_x^{2,3} - I_x^{3,6}) - (I_x^{1,4} - I_x^{4,5})\} \tag{24}$$

$$F_zS^\beta = 2I_z^{2,6} \tag{25}$$

$$2F_yS_x = \sqrt{2}\{(I_y^{2,3} + I_y^{3,6}) + (I_y^{1,4} + I_y^{4,5})\} \tag{26}$$

Hence, these Hamiltonians in the $I = 1$ 6 × 6 space contains rotations in two disjoint 3 × 3 subspaces spanned by {|2⟩, |3⟩, |6⟩} and {|1⟩, |4⟩, |5⟩}, respectively. Using this formulation, U_α^{in} may be recast in the form

$$U_\alpha^{in} = U_bU_a \tag{27}$$

where

$$U_a = e^{i\theta_m 2F_yS_x}e^{i(2\pi/3)F_zS^\beta}e^{-i\theta_m 2F_yS_x}$$

$$= e^{-i(4\pi/3\sqrt{3})(I_x^{2,3}+I_x^{3,6}-I_z^{2,6})} \tag{28}$$

$$U_b = e^{i(\pi/2)S_z}e^{-i(\pi/2)S_z}e^{-i(\pi/2)^2F_yS_y}e^{-i(\pi/2)2F_yS_x}$$

$$= e^{i(\pi/2)S_z}e^{-i(\pi/2)(I_x^{1,5} + (1/2)I^4)}e^{i(\pi/2)(I_x^{2,6}+(1/2)I^3)}$$

$$= e^{i(\pi/2)S_z}e^{i(\pi/2)I_z^{3,4}}\, e^{-i(\pi/2)(I_x^{1,5}-I_x^{2,6})} = e^{i(\pi/2)S_z}U_b^z\, U_b^x \tag{29}$$

with $I^r = |r\rangle\langle r|$. In U_b the S_z rotation may be ignored as it communtes with the target state, so what is left are three commuting two-level rotations. On the other hand, description of the evolution under U_a in the {|2⟩, |3⟩, |6⟩} subspace requires the transformation formulas

$$UI_{5,6}^-U^\dagger = \alpha I_{5,6}^- + \beta I_{5,3}^- + \gamma I_{5,2}^- \tag{30}$$

$$UI_{3,4}^-U^\dagger = -\beta I_{2,4}^- + \delta I_{3,4}^- + \beta^* I_{6,4}^- \tag{31}$$

$$UI_{1,2}^-U^\dagger = \alpha^* I_{1,2}^- - \beta^* I_{1,3}^- + \gamma I_{1,6}^- \tag{32}$$

where $U = e^{-i\phi(I_x^{2,3} + I_x^{3,6} - I_z^{2,6})}$ and $\alpha = \delta - \kappa$, $\beta = \gamma - \kappa$, $\gamma = -^2/_3 \sin^2\theta$, and $\delta = {}^2/_3 \cos^2\theta$ with $\kappa = (i/\sqrt{3})\sin 2\theta$ and $\theta = (\sqrt{3}/2)\phi$. The cumulative effect of U_a, U_b^x, and U_b^z in transformation of the individual coherences of S^- into $I_1^-I_2^\alpha + I_1^\alpha I_2^-$ is illustrated by the energy-level diagrams in Figure 1b. Diagrams illustrating the overall effect of U_α^{anti} in the $2F_zS^- \rightarrow I_1^-I_2^\alpha + I_1^\alpha I_2^-$ transformation are given in Figure 1a.

3. Sensitivity and Resolution

The sensitivity and effective resolution of the antiphase and in-phase COS^3 HSQC experiments relative to previous S^3 (α&β HSQC) and COS HSQC experiments (all using PFG) can be evaluated using a J doublet of Lorentzian lines characterized by the frequency-dependent relative signal-to-noise function

$$\mathrm{rSNR}(\nu) = \frac{|b(U)|}{\sqrt{2}}\Delta\nu_{1/2}{}^2\left(\frac{1}{\Delta\nu_{1/2}{}^2 + 4(\nu - J/2)^2} + \frac{1}{\Delta\nu_{1/2}{}^2 + 4(\nu + J/2)^2}\right) \tag{33}$$

arbitrarily normalized relative to the maximum signal-to-noise ratio of the antiphase COS^3 experiment. $|b(U)|$ denotes the norm of the transfer amplitude of the actual experiment being 1, $1/\sqrt{2}$, and $\sqrt{2}$ for the antiphase S^3,[11] COS,[7,10] and COS^3 experiments, respectively, while it is $3\sqrt{6}/16$ and $1/\sqrt{2}$ for the corresponding in-phase COS^{10} and COS^3 experiments. The full doublet, for which each line is characterized by a line width (full width at half-height) $\Delta\nu_{1/2}$, applies for the COS experiments while only one of the lines is relevant for the COS^3 and S^3 experiments. In the former case the maximum peak height corresponds to the frequency $\nu = \pm\,{}^1/_2\sqrt{-\Delta\nu_{1/2}{}^2 - J^2 + 2|J|\sqrt{\Delta\nu_{1/2}{}^2 + J^2}}$ and 0 for $\Delta\nu_{1/2}$ less than or larger than $\sqrt{3}|J|$, respectively. It is noted that eq 33 does not take into account the effects of pulse imperfections and relaxation during the mixing sequences which are most severe for COS^3. Using a value of $J = -14$ Hz for a geminal H−H coupling, this leads to the rSNR versus $\Delta\nu_{1/2}$ curves in Figure 3a,b for the various COS, S^3, and COS^3 pulse sequences for antiphase and in-phase transfer, respectively. The spin-state-selective methods have been divided into categories corresponding to sampling of only one of the two lines (α or β, $I-S$ correlation alone) or both lines (α and β in separate experiments, $I-S$ correlation and measurement of J). Taking into account doubling of the experiment time, the latter category is associated

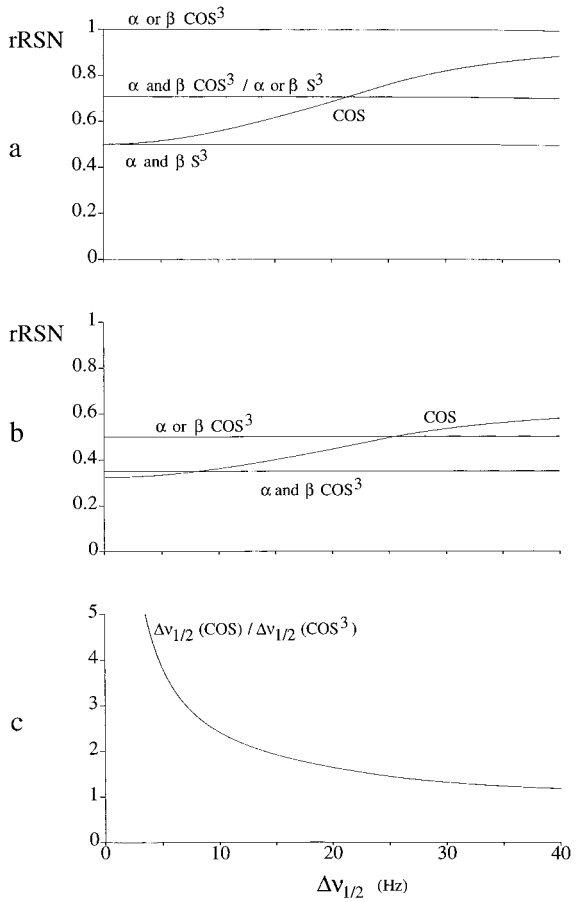

Figure 3. Graphical comparison of (a, b) relative signal-to-noise ratios (rSNR) and (c) resolution for various COS, S^3, and COS^3 pulse sequences for antiphase (a) and in-phase (b) coherence transfer in I_2S spin systems. The rSNR curves correspond to "single-scan", pure-absorption spectra, with "α or β" referring to a single spin-state-selective spectrum with either the α or the β line and "α and β" to the case where both the α and the β spectrum are recorded (rSNR corrected for the doubling of instrument time). In (c) $\Delta\nu_{1/2}(COS^3) = \Delta\nu_{1/2}$ represents the width of a single resonance, while $\Delta\nu_{1/2}$(COS) denotes the overall width of the J doublet.

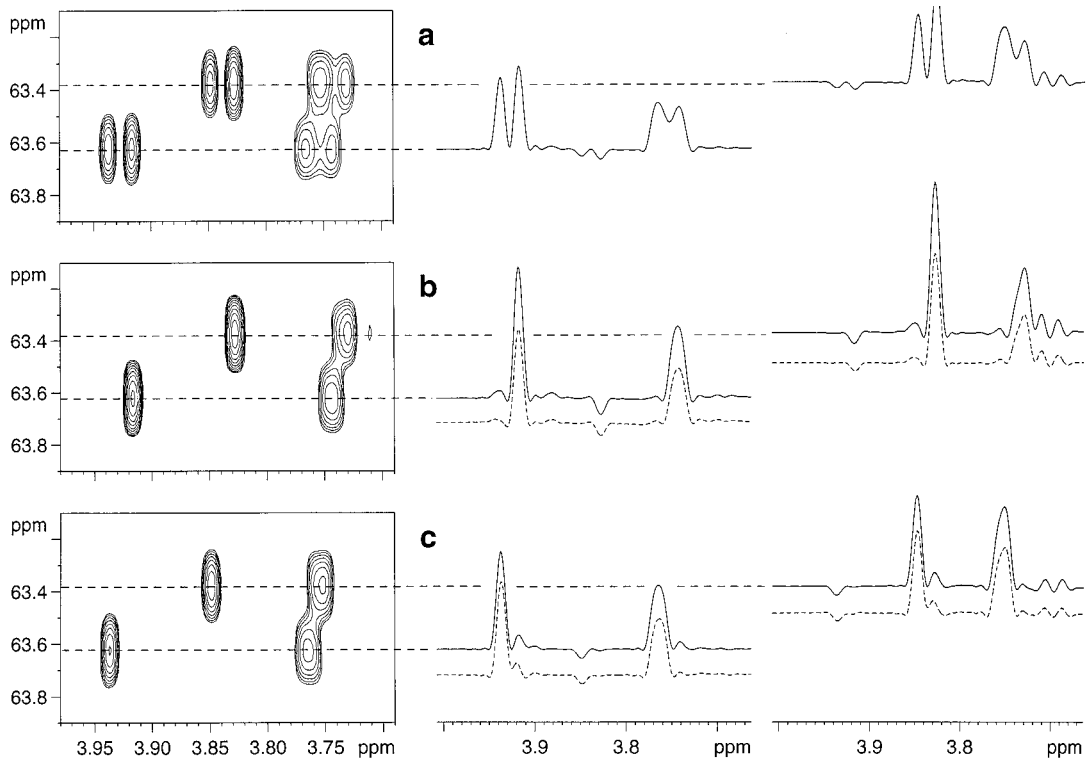

Figure 4. Methylene region of 2D $^{13}C-^{1}H$ correlation spectra of the disaccharide β-*O*-methyl maltoside in D_2O recorded on a Bruker DRX 600 MHz spectrometer. (a) COS H SQC spectrum optimized for I_2S groups.[7] Here each CH_2 group appears as a pair of doublets, with the $\omega_2/2\pi$ sections exhibiting strong-coupling effects. (b, c) COS^3 HSQC spectra selecting the multiplet component with the geminal proton in the α or β state, respectively (pulse sequence in Figure 2a). In the CH_2 groups of β-*O*-methyl maltoside, J_{CH} is 144.3 Hz, implying $\tau_1 = 2.11$ ms, $\tau_2 = 2.31$ ms, $\tau_3 = 1.36$ ms, and $\tau_4 = 3.47$ ms for the COS^3 HSQC sequence in Figure 2a. The sensitivity of the α COS^3 spectrum in b is 39% higher than that in the α HSQC reference experiment[11] represented by dotted lines in the $\omega_2/2\pi$ sections which compares favorably with the theoretical enhancement of 41%. The COS^3 β spectrum (c) shows less gain (7−10%). All of the spectra are recorded with 16 scans with 2048 complex data points in t_2 and 512 increments in t_1; zero-filling to 4096(t_1) × 8192(t_2) complex data points prior to strip transformation; apodization in both dimensions by cosine windows shifted by $\pi/6$; WALTZ-16 decoupling on ^{13}C during t_2. The gradient ratios −80:30:−30:±15.0866 were used for echo/antiecho selection.

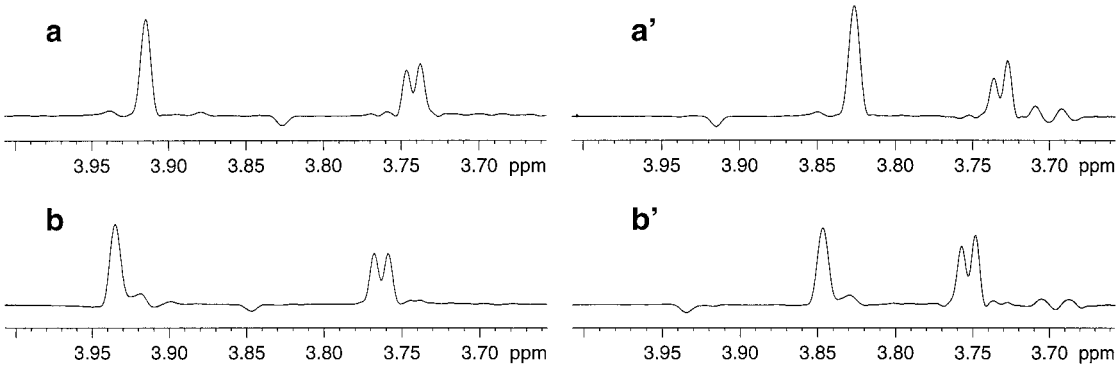

Figure 5. $\omega_2/2\pi$ sections of COS^3 in-phase $^{13}C-^{1}H$ correlation spectra of the methylene group region of β-*O*-methyl maltoside using the pulse sequence of Figure 2b. The $\omega_2/2\pi$ sections in (a, a′) and (b, b′) correspond to the sections in parts b and c of Figure 4, respectively, with a and b referring to the low-field methylene and a′ and b′ to high-field methylene. The experimental parameters are the same as those in Figure 4 except for the initial INEPT transfer replaced by NOE presaturation of approximately 6 s duration (300 proton pulses of 120° separated by delays of 20 ms).

with a decrease in rSNR by a factor of $1/\sqrt{2}$ relative to the former category. We note that for the COS spectra no doublet splittings are visible in the range $\Delta\nu_{1/2} > \sqrt{3}|J|$. Using the same *J* coupling constant, Figure 3c shows the gain in resolution obtained by S^3 and COS^3 (characterized by the width of the α and β line) experiments relative to COS (characterized by the width of the doublet) experiments.

4. Experimental Confirmation

An experimental comparison of COS^3 HSQC with conventional COS HSQC optimized for CH_2 groups[7,10] clearly shows a substantial gain in sensitivity. The experiments were performed on the disaccharide β-*O*-methyl maltoside at 600 MHz proton frequency using the pulse sequences of Figure 2a,b for the antiphase (Figure 4) and in-phase (Figure 5) transfer, respectively. In the conventional antiphase COS spectrum (Figure 4a) each of the two methylene groups appears as a pair of doublets with noticable strong-coupling effects, while they are resolved as a pair of double doublets in the corresponding in-phase spectrum. The COS^3 experiment selects subspectra, with the geminal proton of the CH_2 group being in the α (Figure 4b) or β (Figure 4c) state leading to improved sensitivity and resolution.

However, the enhancement is more pronounced on the α line than on the β line. For the antiphase transfer $2F_zS^- \rightarrow I_1^- I_2^\alpha + I_1^\alpha I_2^-$ the sensitivity gain amounts to some 60% as compared to COS HSQC and 39% compared to α HSQC[11] (dotted line in Figures 4b,c); theory predicts sensitivity gains of 100% and 41%, respectively.

5. Conclusion

We have presented new pulse sequences that reach the unitary bound for the coherence transfers $2F_zS^- \rightarrow I_1^- I_2^{\alpha/\beta} + I_1^{\alpha/\beta} I_2^-$ and $S^- \rightarrow I_1^- I_2^{\alpha/\beta} + I_1^{\alpha/\beta} I_2^-$ for I_2S spin systems. The transfers are both coherence-order- and spin-state-selective. The pulse sequences improve the sensitivity significantly compared to earlier methods, and in conjunction with this, they serve to simplify and improve the resolution of complex spectra by exciting only half the resonances.

Acknowledgment. The use of the spectrometer facilities of the Danish Instrument Center for NMR Spectroscopy of Biological Macromolecules at Carlsberg Laboratory and the computing facilities at the Instrument Centre for Solid-State NMR Spectroscopy at University of Aarhus is acknowledged.

References and Notes

(1) Nielsen, N. C.; Thøgersen, H.; Sørensen, O. W. *J. Am. Chem. Soc.* **1995**, *117*, 11365.

(2) Nielsen, N. C.; Thøgersen, H.; Sørensen, O. W. *J. Chem. Phys.* **1996**, *105*, 3962.

(3) Nielsen, N. C.; Sørensen, O. W. *J. Magn. Reson.* **1996**, *A123*, 135.

(4) Bax, A.; Freeman, R.; Kempsell, S. P. *J. Am. Chem. Soc.* **1980**, *102*, 4849.

(5) Bax, A.; Freeman, R.; Frenkiel, T. A. *J. Am. Chem. Soc.* **1981**, *103*, 2102.

(6) Meissner, A.; Schulte-Herbrüggen, T.; Briand, J.; Sørensen, O. W. *Mol. Phys.* **1998**, *95*, 1137.

(7) Schleucher, J.; Schwendinger, M.; Sattler, M.; Schmidt, P.; Schedletzky, O.; Glaser, S. J.; Sørensen, O. W.; Griesinger, C. *J. Biomol. NMR* **1994**, *4*, 301.

(8) Sattler, M.; Schwendinger, M. G.; Schleucher, J.; Griesinger, C. *J. Biomol. NMR* **1995**, *6*, 11.

(9) Sattler, M.; Schmidt, P.; Schleucher, J.; Schedletzky, O.; Glaser, S. J.; Griesinger, C. *J. Magn. Reson.* **1995**, *B108*, 235.

(10) Untidt, T.; Schulte-Herbrüggen, T.; Luy, B.; Glaser, S. J.; Griesinger, C.; Sørensen, O. W.; Nielsen, N. C. *Mol. Phys.* **1998**, *95*, 787.

(11) Sattler, M.; Schleucher, J.; Schedletzky, O.; Glaser, S. J.; Griesinger, C.; Nielsen, N. C.; Sørensen, O. W. *J. Magn. Reson.* **1996**, *A119*, 171.

(12) Meissner, A.; Duus, J. Ø.; Sørensen, O. W. *J. Magn. Reson.* **1997**, *128*, 92.

(13) Meissner, A.; Duus, J. Ø.; Sørensen, O. W. *J. Biomol. NMR* **1997**, *10*, 89.

(14) Meissner, A.; Schulte-Herbrüggen, T.; Sørensen, O. W. *J. Am. Chem. Soc.* **1998**, *120*, 3803.

(15) Sørensen, M. D.; Meissner, A.; Sørensen, O. W. *J. Biomol. NMR* **1997**, *10*, 181.

(16) Andersson, P.; Annila, A.; Otting, G. *J. Magn. Reson.* **1998**, *133*, 364.

(17) Sørensen, O. W. *Progr. NMR Spectrosc.* **1989**, *21*, 503.

(18) Sørensen, O. W. *J. Magn. Reson.* **1990**, *86*, 435.

(19) Stoustrup, J.; Schedletzky, O.; Glaser, S. J.; Griesinger, C.; Nielsen, N. C.; Sørensen, O. W. *Phys. Rev. Lett.* **1995**, *74*, 2921.

(20) Nielsen, N. C.; Schulte-Herbrüggen, T.; Sørensen, O. W. *Mol. Phys.* **1995**, *85*, 1205.

(21) Glaser, S. J.; Schulte-Herbrüggen, T.; Sieveking, M.; Schedletzky, O.; Nielsen, N. C.; Sørensen, O. W.; Griesinger, C. *Science* **1998**, *280*, 421.

(22) Untidt, T. S.; Glaser, S. J.; Griesinger, C.; Nielsen, N. C. *Mol. Phys.* **1999**, *96*, 1739.

(23) Wokaun, A.; Bodenhausen, G.; Ernst, R. R. *Principles of Nuclear Magnetic Resonance in One and Two Dimensions*; Clarendon Press: Oxford, U.K., 1987.

(24) Wokaun, A.; Ernst, R. R. *J. Chem. Phys.* **1977**, *67*, 1752.

(25) Vega, S. *J. Chem. Phys.* **1978**, *68*, 5518.